



Contents lists available at ScienceDirect

Mechanical Systems and Signal Processing

journal homepage: www.elsevier.com/locate/ymssp



Metamaterial beam with graded local resonators for broadband vibration suppression

Guobiao Hu^a, Andrew C. M. Austin^{b,*}, Vladislav Sorokin^{a,*}, Lihua Tang^a

^a Department of Mechanical Engineering, University of Auckland, 20 Symonds Street, Auckland 1010, New Zealand

^b Department of Electrical, Computer and Software Engineering, University of Auckland, 20 Symonds Street, Auckland 1010, New Zealand



ARTICLE INFO

Article history:

Received 22 December 2019

Received in revised form 9 April 2020

Accepted 13 May 2020

Keywords:

Graded metamaterial

Broadband vibration suppression

Spectral element method

Piezoelectric metamaterial

ABSTRACT

This paper investigates a technique for broadband vibration suppression using a graded metamaterial beam. A series of local resonators with the same mass but different natural frequencies are attached to the beam. The difference between the natural frequencies of neighboring local resonators is defined as the frequency spacing. The spectral element method (SEM) is used to model the graded metamaterial beam, and is verified by the corresponding finite element model (FEM). Three figures of merit are defined to quantitatively evaluate the vibration suppression performance of the proposed metamaterial beam, in terms of the attenuation bandwidth and attenuation strength. Subsequently, a design strategy is proposed, and used to tune the frequency spacing to get a wide attenuation region. A parametric study is conducted to reveal the effects of the frequency spacing and damping ratio on the vibration suppression performance of the graded metamaterial beam: with increasing frequency spacing, the attenuation region first becomes wider, then multiple discrete attenuation regions appear; and with increasing damping ratio, the transmittance response becomes flatter. A piezoelectric metamaterial beam is used to implement the proposed design strategy. Using a synthetic shunt circuit, the 'stiffness' of the local resonator can be tuned using a piezoelectric transducer. The FEM simulation results agree well with the developed theory for the graded metamaterial beam: with tuning of the capacitance spacing (2.4 nF), the attenuation bandwidth can be increased by about 172.8% as compared to the conventional one shunted with identical capacitances.

© 2020 Elsevier Ltd. All rights reserved.

1. Introduction

In recent years, metamaterials with exotic dynamic behaviors, such as negative effective mass [1,2], negative effective stiffness and negative refraction [3,4], have attracted significant research interest. Due to the band gap phenomenon in metamaterials, i.e., in a certain frequency range, wave propagation is forbidden, an important application of metamaterials is for vibration suppression. The band gaps of metamaterials can be easily designed to operate at sub-wavelength frequency ranges [5–7]. However, the application of conventional metamaterials is often significantly limited, since the band gaps are relatively narrow.

To enlarge the band gaps of metamaterials, various approaches have been proposed. For example, using multiple-degree-of-freedom local resonators can lead to multiple band gaps [6,8,9]. This strategy has been implemented for suppressing

* Corresponding authors.

E-mail addresses: a.austin@auckland.ac.nz (A. C. M. Austin), v.sorokin@auckland.ac.nz (V. Sorokin).

vibrations of engineering structures, such as rods [10], beams [11–14] and plates [15]. Attaching multiple independent single-degree-of-freedom local resonators to the main structure can also open multiple band gaps for vibration suppression [16–18]. Similarly, introducing internal couplings between neighboring local resonators in conventional metamaterials can induce additional band gaps [2,19–21]. Hybrid metamaterials with merged Bragg Scattering and local resonance-based band gaps have also been proposed to achieve wider band gaps for broadband vibration suppression [22–24]. Besides the idea of generating multiple band gaps, some researchers have proposed actively tunable metamaterials for strengthening the broadband performance, typically this tunability is achieved using the piezoelectric shunting technique [14,25–29]. The resonance created by the shunt circuit can generate a reaction force and/or moment back onto the mechanical structure through the piezoelectric effect. However, additional power, sensing and feedback control circuits are required for tuning, which increases the implementation complexity. Other strategies to achieve wide band gaps for metamaterials include the use of nonlinearity [30–32]. In particular, Fang *et al.* [31] showed that ultra-broad band gaps can be obtained from nonlinear metamaterials by inducing chaotic motions. For the considered metamaterial consisting of Duffing oscillators with the nonlinearity implemented by magnetic forces, the vibration attenuation bandwidth was increased by two orders of magnitude [31].

The research outlined in the above paragraph largely focused on the analysis of uniform metamaterials embedded with identical local resonators. In contrast, Brennan [33] developed a wideband vibration neutralizer that consists of an array of resonators with slightly different natural frequencies. Both theoretical and experimental results demonstrated that the proposed vibration neutralizer could operate over a wide bandwidth. However, the hosting structure for the neutralizer in [33] was assumed to be a single-degree-of-freedom rigid body, and thus not a *meta*-structure. The concept of using multiple different resonators can also be implemented for metamaterials. Based on this idea, Banerjee *et al.* [34] investigated a graded one-dimensional metamaterial modelled as a lumped mass-spring system with local resonators of varying natural frequencies. With proper tuning of the frequency spacing between the local resonators, the attenuation bandwidth of this graded metamaterial was increased by 40%, compared to a conventional metamaterial with uniform local resonators. However, the mass-spring model used in [34] is purely theoretical, and in many cases is not able to properly describe the dynamics of real structures, such as beams [35] and plates [36,37].

In this paper, a metamaterial beam with graded local resonators is proposed for realizing broadband vibration suppression. “Graded” refers to the variation in the natural frequencies of the local resonators. The mass of each local resonator is assumed to be identical, and the spring stiffness of each local resonator is varied to meet the “graded” condition. The spectral element method (SEM) is used to model the graded metamaterial beam. Several figures of merit have been developed for later quantitative analysis. The SEM results are verified with comparisons against a finite element method (FEM). A design strategy is proposed, and criteria towards the tuning of the frequency spacing between local resonators are derived. A parametric study is performed to investigate the effects of the frequency spacing and damping ratio on the vibration suppression performance of the graded metamaterial beam. The derived design criteria are validated by the parametric study results. Finally, to give an example of the practical implementation of the proposed graded metamaterial beam, a piezoelectric shunt circuit is adopted, and a piezoelectric metamaterial beam is developed. The tuning of local resonators can be realized through the manipulation of the shunt circuits. The electric components that constitute the shunt circuits are realized with synthetic circuits for the ease of tuning. Numerical simulation results show that with carefully tuned shunt circuits, the graded piezoelectric metamaterial beam can feature a significantly wider attenuation bandwidth than the conventional counterpart.

2. Theoretical foundation

2.1. Model formulation

Fig. 1(a) shows an infinitely long model of the conventional metamaterial beam with uniform local resonators attached. **Fig. 1(b)** shows the proposed graded metamaterial beam system with N local resonators attached. The presence of the attached local resonators will be embodied in the continuity conditions for the proposed graded metamaterial beam. Adding a local resonator implies satisfying four equations to guarantee the continuity of displacement, slope, force, and moment at the point of attachment. As the number of local resonators increases, the modelling of this system using analytical methods becomes cumbersome. Using the SEM [38] the entire structure is first divided into subsections, which are simple Euler beams with one resonator attached. After deriving the dynamic stiffness element that describes the relationship between nodal forces and displacements for a single beam subsection, the entire structure can be modelled by assembling the dynamic stiffness matrices of all the elements.

2.1.1. Governing equations

Considering one beam subsection without a local resonator, using Euler beam theory, the governing equation can be expressed:

$$\rho A_{cs} \frac{\partial^2 w(x, t)}{\partial t^2} + EI \frac{\partial^4 w(x, t)}{\partial x^4} = 0 \quad (1)$$

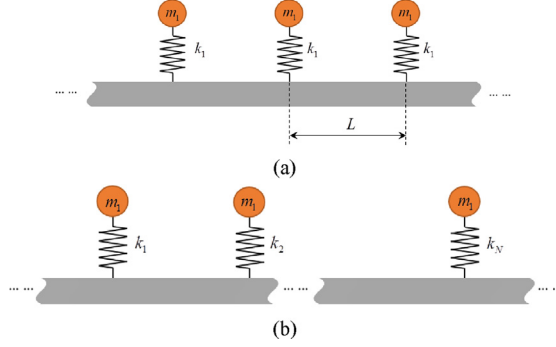


Fig. 1. (a) Infinitely long model of the conventional metamaterial beam with uniform local resonators attached, (b) schematic of the metamaterial beam with graded local resonators attached.

where $w(x, t)$ is the transverse displacement, ρ is the mass density, A_{cs} is the cross-sectional area, E is Young's modulus, and I is the area moment of inertia about the neutral axis. The coupling between the beam and resonators is taken into account by applying the displacement and force continuities at the attachment points of the local resonators later in [Section 2.1.3](#). In this study, we consider masses of all the local resonators to be the same, since for practical engineering, there often exists a weight limit for mechanical structures. As is known, the band gap width produced by a local resonator depends on the mass of the resonator [39]. Thus, although arbitrarily increasing the mass of the local resonator will increase the band gap width, such an approach may be not relevant from practical point of view. For the above reasons, only the spring stiffnesses of the local resonators are varied to meet the “graded” condition. The equation of motion for the j^{th} local resonator is expressed as:

$$m\ddot{u}_j(t) + c_j(\dot{u}_j(t) - \dot{w}(x_j, t)) + k_j(u_j(t) - w(x_j, t)) = 0 \quad (2)$$

where $u_j(t)$ is the absolute displacement of the j^{th} local resonator, and m , c_j and k_j are the mass, damping coefficient and stiffness respectively. A constant frequency spacing, δ , between the natural frequencies of the neighboring local resonators is introduced and is the same for all the values of j . Actually, removing the restriction of constant frequency spacing, δ , could be beneficial for the performance of the metamaterial, but the corresponding analysis is not within the scope of this paper, since our aim is to show that the graded metamaterial with properly chosen constant frequency spacing can outperform the conventional metamaterial. An expression for δ is

$$\delta = \frac{(\omega_j - \omega_1)}{\omega_1(j-1)} \quad (3)$$

where $j = 2, 3, \dots, N$. Thus, k_j and c_j can be expressed in terms of k_1 and c_1 :

$$\begin{cases} k_j = k_1(1 + (j-1)\delta)^2 \\ c_j = c_1(1 + (j-1)\delta) \end{cases} \quad (4)$$

where k_1 and c_1 are the stiffness and damping coefficient of the first local resonator.

2.1.2. Non-Dimensionlization

To generalize the analysis presented in this study, the governing equations are non-dimensionalized to take the form:

$$\begin{cases} \frac{\partial^2 \tilde{w}}{\partial \tilde{t}^2} + \frac{\mu}{\alpha} \frac{\partial^4 \tilde{w}}{\partial \tilde{x}^4} = 0 \\ \ddot{u}_j(t) + 2\zeta(1 + (j-1)\delta)(\dot{u}_j(t) - \dot{\tilde{w}}(x_j, t)) + (1 + (j-1)\delta)^2(\tilde{u}_j(t) - \tilde{w}(x_j, t)) = 0 \end{cases} \quad (5)$$

with the following dimensionless parameters used:

$$\mu = \frac{m}{\rho A_{cs} L}; \alpha = k_1 / \left(\frac{EI}{L^3} \right); \tilde{t} = \omega_1 t; \tilde{w} = w/L; \tilde{u} = u/L; \tilde{x} = x/L; \zeta = \frac{c_1}{2\sqrt{mk_1}}; \Omega = \omega/\omega_1$$

where L is the length of a single beam subsection, and $\omega_1 = \sqrt{k_1/m}$ is the natural frequency of the first local resonator. For simplicity, the damping ratios for all the resonators are assumed to be the same and equal to ζ . The non-dimensional shear force and moment are:

$$\begin{aligned}\tilde{M} &= \frac{\tilde{M}}{\left(\frac{EI}{L}\right)} = \frac{\partial^2 \tilde{w}}{\partial x^2} \\ \tilde{V} &= \frac{\tilde{V}}{\left(\frac{EI}{L^2}\right)} = -\frac{\partial^3 \tilde{w}}{\partial x^3}\end{aligned}\quad (6)$$

2.1.3. Spectral element method

Assuming the solution to the first equation of Eq. (5) has the form

$$\tilde{w}(x, t) = \tilde{W}(x; \Omega) e^{i\Omega t} \quad (7)$$

Substituting Eq. (7) into Eq. (5) transforms the governing equation from the time domain into the frequency domain:

$$\frac{\mu}{\alpha} \frac{\partial^4 \tilde{W}}{\partial x^4} - \Omega^2 \tilde{W} = 0 \quad (8)$$

The general solution to Eq. (8) can be expressed:

$$\tilde{W}(x, \Omega) = A_1 e^{-i\beta x} + A_2 e^{-\beta x} + A_3 e^{-i\beta(1-x)} + A_4 e^{-\beta(1-x)} \quad (9)$$

where $\beta = \sqrt{\Omega}(\alpha/\mu)^{1/4}$ is the dimensionless wavenumber. The nodal displacements of the spectral element can thus be expressed in matrix form:

$$\begin{bmatrix} \tilde{W}_1 \\ \tilde{\Theta}_1 \\ \tilde{W}_2 \\ \tilde{\Theta}_2 \end{bmatrix} = \underbrace{\begin{bmatrix} 1 & 1 & e^{-i\beta} & e^{-\beta} \\ -i\beta & -\beta & i\beta e^{-i\beta} & \beta e^{-\beta} \\ e^{-i\beta} & e^{-\beta} & 1 & 1 \\ -i\beta e^{-i\beta} & -\beta e^{-\beta} & i\beta & \beta \end{bmatrix}}_H \begin{bmatrix} A_1 \\ A_2 \\ A_3 \\ A_4 \end{bmatrix} \quad (10)$$

As shown in Fig. 2, the dimensionless nodal forces can be expressed as:

$$\begin{aligned}\tilde{M}_1 &= -\frac{\partial^2 \tilde{W}}{\partial x^2} \Big|_{x=0} ; \quad \tilde{M}_2 = \frac{\partial^2 \tilde{W}}{\partial x^2} \Big|_{x=1} \\ \tilde{V}_1 &= -\frac{\partial^3 \tilde{W}}{\partial x^3} \Big|_{x=0} ; \quad \tilde{V}_2 = \frac{\partial^3 \tilde{W}}{\partial x^3} \Big|_{x=1}\end{aligned}\quad (11)$$

Substituting Eq. (9) into Eq. (11) and rearranging in the matrix form gives:

$$\begin{bmatrix} \tilde{V}_1 \\ \tilde{M}_1 \\ \tilde{V}_2 \\ \tilde{M}_2 \end{bmatrix} = \begin{bmatrix} -i\beta^3 & \beta^3 & i\beta^3 e^{-i\beta} & -\beta^3 e^{-\beta} \\ \beta^2 & -\beta^2 & \beta^2 e^{-i\beta} & -\beta^2 e^{-\beta} \\ i\beta^3 e^{-i\beta} & -\beta^3 e^{-\beta} & -i\beta^3 & \beta^3 \\ -\beta^2 e^{-i\beta} & \beta^2 e^{-\beta} & -\beta^2 & \beta^2 \end{bmatrix} \begin{bmatrix} A_1 \\ A_2 \\ A_3 \\ A_4 \end{bmatrix} \quad (12)$$

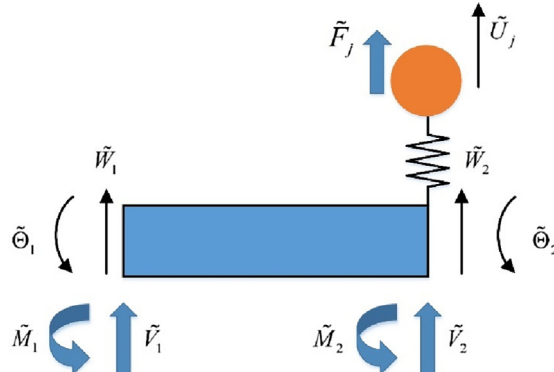


Fig. 2. Spectral element of metamaterial beam.

Combining Eq. (11) and Eq. (12) to express the nodal forces by the nodal displacements leads to:

$$\begin{bmatrix} \tilde{V}_1 \\ \tilde{M}_1 \\ \tilde{V}_2 \\ \tilde{M}_2 \end{bmatrix} = \underbrace{\begin{bmatrix} -i\beta^3 & \beta^3 & i\beta^3 e^{-i\beta} & -\beta^3 e^{-\beta} \\ \beta^2 & -\beta^2 & \beta^2 e^{-i\beta} & -\beta^2 e^{-\beta} \\ i\beta^3 e^{-i\beta} & -\beta^3 e^{-\beta} & -i\beta^3 & \beta^3 \\ -\beta^2 e^{-i\beta} & \beta^2 e^{-\beta} & -\beta^2 & \beta^2 \end{bmatrix}}_{S_B(\omega)} H^{-1} \begin{bmatrix} \tilde{W}_1 \\ \tilde{\Theta}_1 \\ \tilde{W}_2 \\ \tilde{\Theta}_2 \end{bmatrix} \quad (13)$$

in which H is defined in Eq. (10) and $S_B(\omega)$ can be explicitly obtained as:

$$S_B(\omega) = \begin{bmatrix} \Gamma_1 & \bar{\Gamma}_3 & -\bar{\Gamma}_1 & \Gamma_3 \\ \Gamma_2 & -\Gamma_3 & \bar{\Gamma}_2 & \\ \Gamma_1 & -\bar{\Gamma}_3 & & \\ sym & & \Gamma_2 & \end{bmatrix} \quad (14)$$

where the subscript B denotes the beam and

$$\begin{aligned} \Gamma_1 &= (\cos\beta\sinh\beta + \sin\beta\cosh\beta)\beta^3/(1 - \cos\beta\cosh\beta) \\ \Gamma_2 &= (-\cos\beta\sinh\beta + \sin\beta\cosh\beta)\beta/(1 - \cos\beta\cosh\beta) \\ \Gamma_3 &= (-\cos\beta + \cosh\beta)\beta^2/(1 - \cos\beta\cosh\beta) \\ \bar{\Gamma}_1 &= (\sin\beta + \sinh\beta)\beta^3/(1 - \cos\beta\cosh\beta) \\ \bar{\Gamma}_2 &= (-\sin\beta + \sinh\beta)\beta/(1 - \cos\beta\cosh\beta) \\ \bar{\Gamma}_3 &= (\sin\beta\sinh\beta)\beta^2/(1 - \cos\beta\cosh\beta) \end{aligned}$$

For the j^{th} local resonator, the solution to the second equation of (5) is assumed to have the form:

$$\tilde{u}(\tilde{x}, \tilde{t}) = U(\tilde{x}; \Omega) e^{i\Omega\tilde{t}} \quad (15)$$

Similarly, by substituting Eqs. (7) and (15) into Eq. (5), the frequency domain form of the governing equation of the local resonator can be obtained:

$$-\Omega^2 \tilde{U}_j(\Omega) + 2i\Omega(1 + (j-1)\delta)\zeta \left(\tilde{U}_j(\Omega) - \tilde{W}(x_j, \Omega) \right) + (1 + (j-1)\delta)^2 \left(\tilde{U}_j(\Omega) - \tilde{W}(x_j, \Omega) \right) = 0 \quad (16)$$

Deliberately dividing the host beam into subsections at the attachment points of local resonators, we obtain the representative spectral element of the metamaterial beam (Fig. 2), and considering the displacement continuity, we have $\tilde{W}(x_j, \Omega) = \tilde{W}_{2,j}$. The subscript j denotes the j^{th} metamaterial beam element. The reacting force applied by the j^{th} local resonator onto the beam is:

$$\tilde{F}_R = -\left(\Gamma_{5j} \tilde{W}_{2,j} - \Gamma_{5j} \tilde{U}_j \right) \quad (17)$$

where $\Gamma_{5j} = \alpha \begin{bmatrix} (1 + (j-1)\delta)^2 \\ +2i\Omega(1 + (j-1)\delta)\zeta \end{bmatrix}$. Considering the force continuity at the attachment point, one obtains:

$$\tilde{V}_{2,j} = -\bar{\Gamma}_1 \tilde{W}_{1,j} - \Gamma_3 \tilde{\Theta}_{1,j} + (\Gamma_1 + \Gamma_{5j}) \tilde{W}_{2,j} - \bar{\Gamma}_3 \tilde{\Theta}_{2,j} \tilde{W}_{2,j} - \Gamma_{5j} \tilde{U}_j \quad (18)$$

The dynamic stiffness matrix of the j^{th} metamaterial beam element with the local resonator can thus be derived as:

$$S_{MBj}(\omega) = \begin{bmatrix} \Gamma_1 & \bar{\Gamma}_3 & -\bar{\Gamma}_1 & \Gamma_3 & 0 \\ \Gamma_2 & -\Gamma_3 & \bar{\Gamma}_2 & 0 & \\ \Gamma_1 + \Gamma_{5j} & -\bar{\Gamma}_3 & -\Gamma_{5j} & & \\ sym & & \Gamma_2 & 0 & \\ & & & \Gamma_{4,j} & \end{bmatrix} \quad (19)$$

where the subscript MB denotes the metamaterial beam, $\Gamma_{4,j} = \alpha \begin{bmatrix} (1 + (j-1)\delta)^2 - \Omega^2 \\ +2i\Omega(1 + (j-1)\delta)\zeta \end{bmatrix}$. The corresponding nodal displacement vector is:

$$[d_{MB,j}] = \begin{bmatrix} \tilde{W}_{1,j} & \tilde{\Theta}_{1,j} & \tilde{W}_{2,j} & \tilde{\Theta}_{2,j} & \tilde{U}_j \end{bmatrix}^T \quad (20)$$

After obtaining the spectral element, the assembly of the model for the whole system (i.e., the finitely long model containing N local resonators) is similar to the conventional finite element model: the global equation is developed by assembling the element matrices; the boundary conditions are applied; the displacement frequency responses are derived. In this study the left-hand side of the beam is clamped, and the base excitation is applied at this side of the beam. The right-hand side of the beam is under the ‘free’ condition. The transmittance of the metamaterial beam is defined as follows:

$$\tau(\Omega) = \frac{|\tilde{W}_{2,N}(\Omega)|}{|\tilde{W}_{1,1}(\Omega)|} \quad (21)$$

which is the ratio between the displacement amplitude of the free end (i.e., the right-hand side of the N^{th} spectral element) to that of the base. A value of $\tau(\Omega) < 1$ means the vibration amplitude of the free end is smaller than that of the base, implying the vibration is attenuated.

2.2. Method verification

In this section, the SEM model is verified through a comparison with the corresponding FEM solution developed using ANSYS. Fig. 3(a) and (b) show the transmittance of conventional and graded metamaterial beams, respectively, calculated using SEM and FEM. The verification model consists of a host beam with 6 local resonators: the length, width and thickness of the host beam are 600 mm, 20 mm and 2 mm, respectively. For the conventional metamaterial beam, the parameters of the 6 identical local resonators are: the resonator mass m is 20 g, the natural frequency is 90 Hz, and the damping ratio is 0.005. For the graded metamaterial beam, all the resonator masses are kept the same, with damping ratios 0.005. The natural frequencies of the 1st to 6th resonators are: 90, 95, 100, 105, 110, 115 Hz.

For the finite element model, the host beam is modelled using the BEAM188 element and the local resonator is modelled using the combination of the MASS21 and COMBIN14 elements. Each subsection of the host beam is meshed with 80 elements to ensure convergence, with a total of 480 elements for the entire host beam. In comparison, the spectral element method only requires 6 elements for modelling the same metamaterial beam. Fig. 3 shows that the results from SEM are in good agreement with those from FEM.

2.3. Figures of merit

Several figures of merit are established to evaluate the vibration suppression performance of the proposed metamaterial beam. First, the dominant attenuation bandwidth Ω_D is defined

$$\Omega_D = \max(|\Im|), \{ \forall \Omega \ni \Im, 20\log(\tau(\Omega)) < 0 \} \quad (22)$$

which measures the largest bandwidth in the attenuation region $20\log(\tau(\Omega)) < 0$ dB. Besides the bandwidth, the value of attenuation within this region is also important. A smaller $\tau(\Omega)$ indicates a stronger attenuation. The minimum attenuation

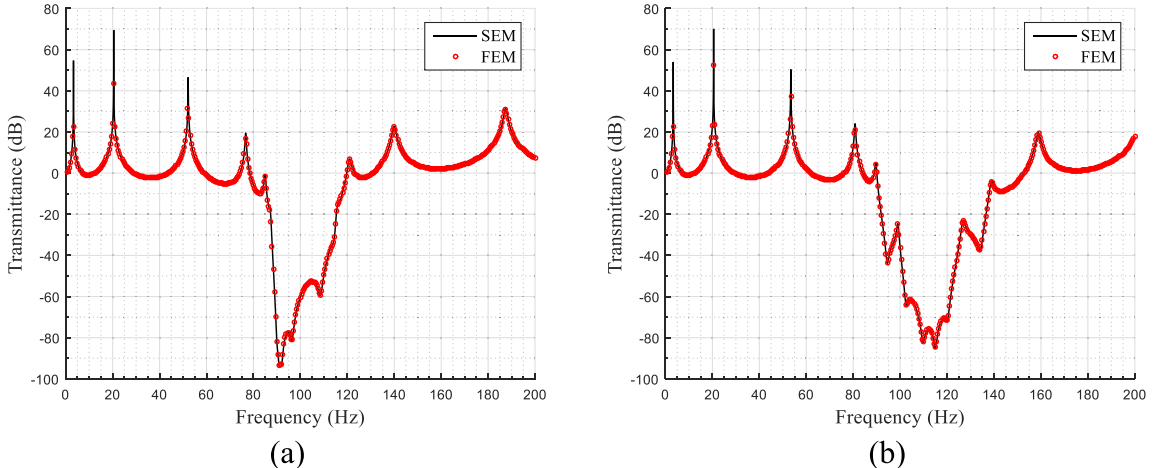


Fig. 3. Transmittances calculated by the spectral element method and finite element method: (a) conventional metamaterial beam; (b) graded metamaterial beam.

index τ_{\min} represents the maximum attenuation strength of the metamaterial over a specific frequency range $[\Omega_A, \Omega_B]$ and is defined

$$\tau_{\min} = \min\{20\log(\tau(\Omega)), \Omega_A \leq \Omega \leq \Omega_B\} \quad (23)$$

However, in circumstances where the vibration energy is spread over a wide spectrum, e.g., a white-noise excitation, enhancing the average attenuation over the entire frequency range of interest is of greater importance. To this end, the averaged attenuation index τ_{avg} gives a measure of the overall attenuation strength of the metamaterial system over the desired frequency range (i.e., $[\Omega_A, \Omega_B]$) and is defined

$$\tau_{avg} = 20\log \left[\int_{\Omega_A}^{\Omega_B} \tau(\Omega) d\Omega \right] \quad (24)$$

3. Design strategy

The band gap width (denoted by Δ) of the conventional metamaterial beam with attached uniform local resonators (i.e., Ω_1) is [40]:

$$\Delta = (\sqrt{1+\mu} - 1)\Omega_1 \quad (25)$$

Eq. (25) is obtained assuming an infinitely long undamped model. For a practical metamaterial system containing only a limited number of cells, the effective attenuation frequency range can be narrower than Δ . By intentionally varying the natural frequency spacing δ , and making each resonator operate in different (but overlapped) frequency ranges, it may be possible to achieve an overlapped wide attenuation region. If δ is large, multiple discrete attenuation regions introduced by different local resonators may appear. For broadband vibration suppression, the former case is more favorable. Therefore, it is important to investigate the criteria for tuning δ to generate an overlapped wide attenuation region rather than multiple discrete attenuation regions. By regarding the first local resonator as the reference, i.e., with the natural frequency $\Omega_1 = 1$, we can define two different configurations for the graded metamaterial beam, depending on the arrangement of the graded local resonators. For the case when the local resonators are arranged in the ascending order, i.e., $\Omega_1 < \dots < \Omega_N$, the first local resonator generates the narrowest band gap. To prevent discrete attenuation regions, it is straightforward to deduce the criterion for avoiding overtuning δ :

$$\delta < \Delta = \delta_u \quad (26)$$

where the subscript u denotes the upper bound of the frequency spacing. For the case where the local resonators are arranged in descending order, i.e., $\Omega_1 > \dots > \Omega_N$, the N^{th} local resonator generates the narrowest band gap $\Delta_N = \Delta[1 + (N-1)\delta]$, note that δ is negative in this case. To ensure $|\delta|$ is smaller than the narrowest band gap Δ_N , one obtains:

$$\delta > -\frac{\Delta}{[1 + (N-1)\Delta]} = \delta_l \quad (27)$$

where the subscript l denotes the lower bound of the frequency spacing. Criterions are proposed as necessary (but possibly insufficient conditions) to ensure an overlapped wide attenuation region for the proposed graded metamaterial beam. It is worth noting that since Eq. (25) is obtained for an undamped metamaterial, the aforementioned criterions are proposed under undamped or small damping condition. In fact, damping plays an important role in affecting the system dynamic responses. Chen et al. [41] reported a metadamping phenomenon and pointed out that introducing dissipative components into metamaterials can improve the vibration attenuation performance. The results showed that two discrete band gaps can be merged to form a broadband frequency range for vibration attenuation by tuning the damping. Based on a similar mechanism presented in [41], it is reasonable to expect that discrete attenuation regions can be merged in the proposed graded metamaterial by introducing appropriate system damping. In the following study (Section 4.2), we will use this idea to merge discrete attenuation regions for broadening the frequency range of vibration attenuation.

It is also worth mentioning that instead of non-uniform local resonators, non-uniform spatial spacing between the local resonators could be beneficial for vibration attenuation, due to the Anderson localization phenomenon [42]. However, for the lower frequency range considered in the paper (when the wavelength is much larger than the spatial spacing between the local resonators), the actual spatial distribution of the resonators can have only minor effect on the performance of the metamaterial [43]. For higher frequencies, the Anderson localization phenomenon [42] induced by the irregular spatial spacing between the local resonators could be beneficial for vibration attenuation.

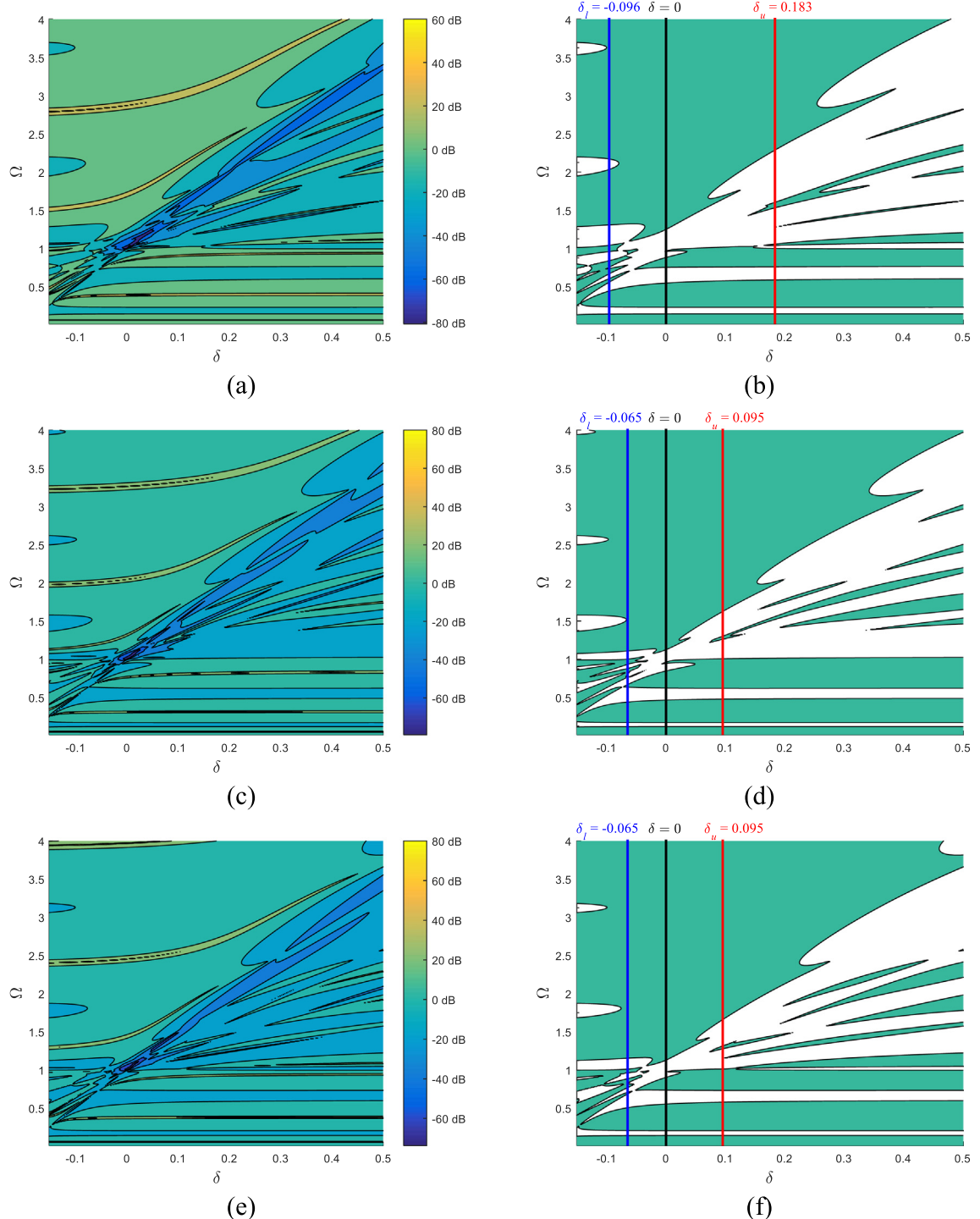
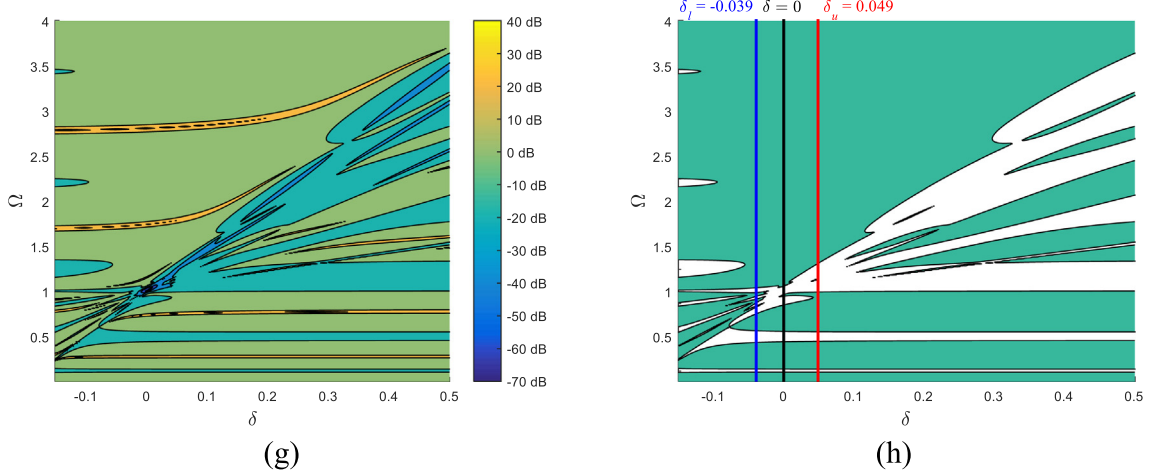


Fig. 4. (a),(c),(e),(g) Contour representation of the transmittance pattern evolution in response to the variation of δ , (b),(d),(f),(h) image binarization using 0 dB as reference. (a) and (b): $\mu = 0.4$ & $\alpha = 0.6$; (c) and (d): $\mu = 0.2$ & $\alpha = 0.6$; (e) and (f): $\mu = 0.2$ & $\alpha = 0.4$; (g) and (h): $\mu = 0.1$ & $\alpha = 0.4$.

**Fig. 4 (continued)**

4. Parametric study

4.1. Effect of the natural frequency spacing δ

This subsection is devoted to investigating the effect of the natural frequency spacing δ on the vibration suppression performance of the graded metamaterial beam. Without loss of generality, in the following case studies, we consider a metamaterial beam with 6 local resonators attached.

For the graded metamaterial beam with the mass ratio $\mu = 0.4$ and non-dimensional stiffness of the resonator $\alpha = 0.6$, Fig. 4(a) presents the evolution of the transmittance pattern in response to variation in δ . By selecting 0 dB as the reference to make a distinction between the attenuated and unattenuated regions, Fig. 4(b) is obtained by a binarization of Fig. 4(a). The unshaded area denotes the attenuation region, i.e., the region where the transmittance is reduced below 0 dB. It should be noted that $\delta = 0$ corresponds to the case of the conventional metamaterial beam with uniform local resonators attached.

It is observed that when $\delta = 0$, the main attenuation region is in the vicinity of $\Omega = 1$, which is well known from the band gap generation mechanism of locally resonant metamaterials. It is observed that as δ increases above 0, the attenuation region first becomes wider, then multiple discrete attenuation regions appear. The multiple discrete attenuation regions appear in the higher frequency range, since $\delta > 0$ implies the natural frequencies of the local resonators are tuned in the ascending order. For $\delta < 0$, similar behavior is observed: with increasing natural frequency spacing $|\delta|$, the dominant attenuation region first becomes wider, then multiple discrete attenuation regions appear. An important difference for $\delta < 0$ is that the attenuation regions move into the lower frequency range.

In Fig. 4(b), the critical values of δ (i.e., δ_l & δ_u) as defined in Section 3.1 are indicated. It is observed that beyond $(-0.096, 0.183)$, multiple fractured attenuation regions always appear, confirming the speculation in Section 3.1. Eqs. (26) and (27) are two necessary conditions to guarantee the generation of an overlapped wide attenuation region. Fig. 4(c)–(h) show cases with different μ and α . It is observed that as δ increases, the trends of the transmittance pattern with different μ and α are similar. The conclusions obtained from Fig. 4(a) and (b) regarding the tuning of δ for achieving an overlapped attenuation region are still valid for other cases.

To further understand how the transmittance pattern varies with δ , a slice view of Fig. 4(a) is presented in Fig. 5 which shows the transmittance responses of the metamaterial beam system for a series of discrete δ . With increasing $|\delta|$ (for $\delta < 0$), the attenuation regions in the transmittance pattern move toward a lower frequency range when compared to the conventional metamaterial (i.e., $\delta = 0$). It is observed that $\delta < 0$ always deteriorates the maximum attenuation strength of the metamaterial beam system, as qualitatively illustrated in Fig. 5(a) by the depths of the valleys in the transmittance pattern. For $\delta > 0$, the width of the dominant attenuation region increases, while the maximum attenuation strength is slightly weakened. Moreover, a large natural frequency spacing (i.e., $|\delta|$) results in several discrete attenuation regions, with the dominant one situated in the high-frequency range. This is unfavorable from the perspective of low-frequency broadband vibration suppression. Therefore, to balance the demands of an overlapped wide attenuation region and satisfactory attenuation strength, it is inferred there exists an optimal δ to meet this trade-off.

In the following parametric study, the effort is devoted to determining the optimal δ . The analysis from Fig. 4 gives a comprehensive but coarse view of the evolution of the transmittance pattern with changing δ . Similarly, the discussion related to Fig. 5 qualitatively explains how the dominant attenuation region varies in terms of the bandwidth. As both bandwidth (i.e., Ω_D) and attenuation strength (i.e., τ_{min} & τ_{avg}) are of importance, the following analysis devotes more efforts into a quantitative investigation.

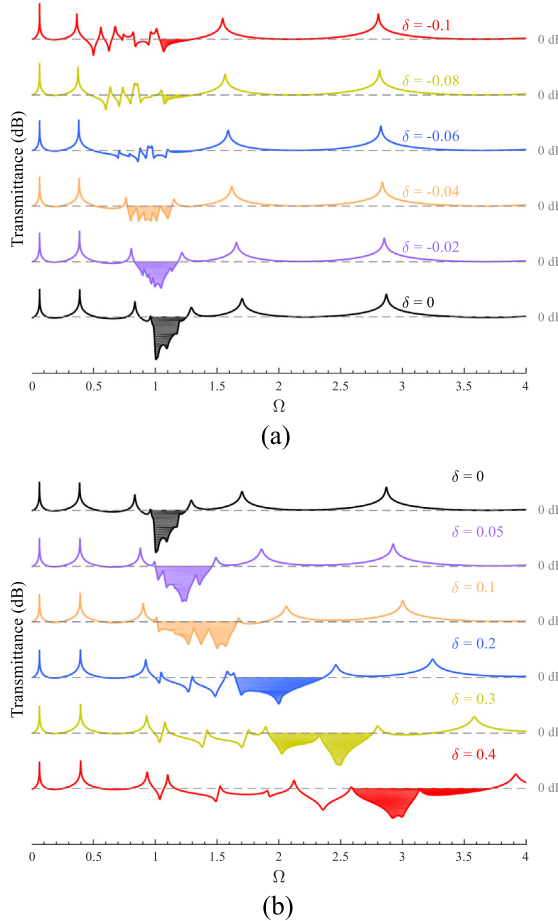


Fig. 5. Transmittance responses of the metamaterial beam with $\mu = 0.4$ & $\alpha = 0.6$ for different δ . The color-filled area denotes the dominant attenuation region.

With changing δ , Fig. 6(a)–(c) demonstrate the evolution of transmittance pattern for the proposed metamaterial beam, focusing only on the dominant attenuation region based on a quantitative analysis using the figures of merit established in Section 2.3. It is noted that the curves presented in Fig. 6(a)–(c) are not smooth. As can be seen from Fig. 4(b) for the same parameters, the boundaries of the dominant attenuation region change non-smoothly. This will be the case for any parameters of the system, since increasing δ leads to fracturing the dominant attenuation region.

It is observed in Fig. 6(a), that the maximum bandwidth of the dominant attenuation region Ω_D occurs at $\delta = 0.14$. While further increasing δ appears to increase the attenuation regions, the main contribution comes only from the high-frequency range, which brings no benefit for low-frequency vibration suppression.

Considering the demand for low-frequency vibration suppression, the evolution of the lower bound for the dominant attenuation region is analyzed. With increasing δ in Fig. 6(b), the lower bound almost monotonically increases, which is undesirable for low-frequency vibration suppression. Making $\delta < 0$ (i.e., arranging the local resonators in the descending order), the lower bound decreases. Moreover, it is worth noting there exists a specific value of δ where the proposed metamaterial system produces a dominant attenuation region with the lowest starting frequency. Fig. 7 shows an example of the transmittance response of the graded metamaterial beam with $\delta = -0.0575$.

Fig. 6(c) presents τ_{\min} and τ_{avg} for the dominant attenuation region with varying δ . The frequency range of interest (i.e., $[\Omega_A, \Omega_B]$) is the dominant attenuation region that can be determined from Fig. 6(b). It is observed that for τ_{\min} , a small deviation from $\delta = 0$ gives the maximum attenuation strength. Prior to this parametric study, it was expected that a conventional metamaterial beam with uniform local resonators distributed ($\delta = 0$) would produce the largest $|\tau_{\min}|$. Fig. 7 gives a comparison between the transmittance responses for these two cases: the conventional uniform design $\delta = 0$, and the graded design with $\delta = 0.00625$. According to the authors' knowledge, no existing literature has identified this phenomenon. In [33], the proposed vibration neutralizer consisting of multiple resonators tuned to different natural frequencies was studied, and the optimal spacing between the natural frequencies of the resonators to achieve the best performance was found to be half the damping ratio. However, the conclusion drawn from [33] obviously does not suit the current case, since in the case of

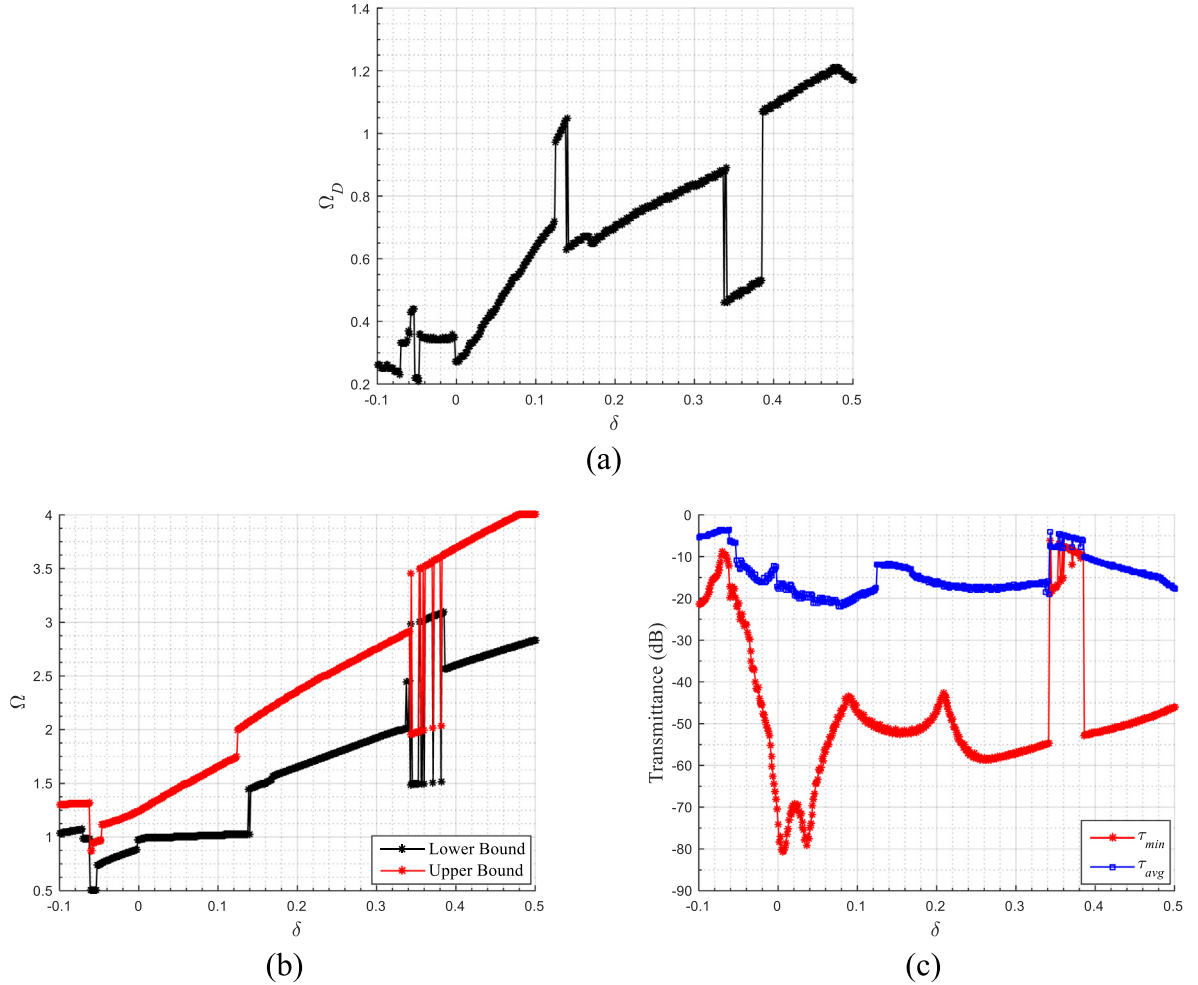


Fig. 6. Evolutions of (a) the bandwidth of the dominant attenuation region, Ω_D , (b) lower and upper bounds of the dominant attenuation region, (c) attenuation indexes (τ_{min} & τ_{avg}) of the dominant attenuation region with the change of δ , for the graded metamaterial beam with $\mu = 0.4$ & $\alpha = 0.6$.

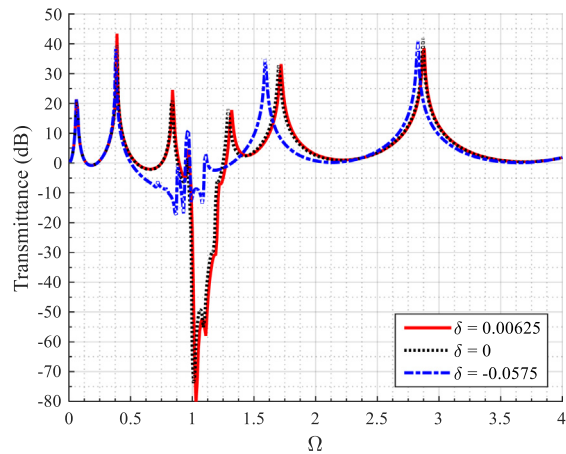


Fig. 7. Transmittance responses of the graded metamaterial beam with $\mu = 0.4$ & $\alpha = 0.6$, at $\delta = 0.00625$, $\delta = 0$ and $\delta = -0.0575$.

Fig. 7, the damping ratio is $\zeta = 0.005$. Since the focus of the current study is on widening the attenuation region rather than enhancing the attenuation strength, efforts will be devoted to exploring the in-depth physical explanation on this phenomenon in a prospective study.

As shown in **Fig. 6(c)**, the variation of δ does not have a significant influence on τ_{avg} . The optimal τ_{avg} is obtained not at $\delta = 0$, but for positive δ . Based on this quantitative analysis, the proposed metamaterial beam with tuned graded local resonators ($\delta \neq 0$) can outperform a conventional counterpart with uniform local resonators ($\delta = 0$).

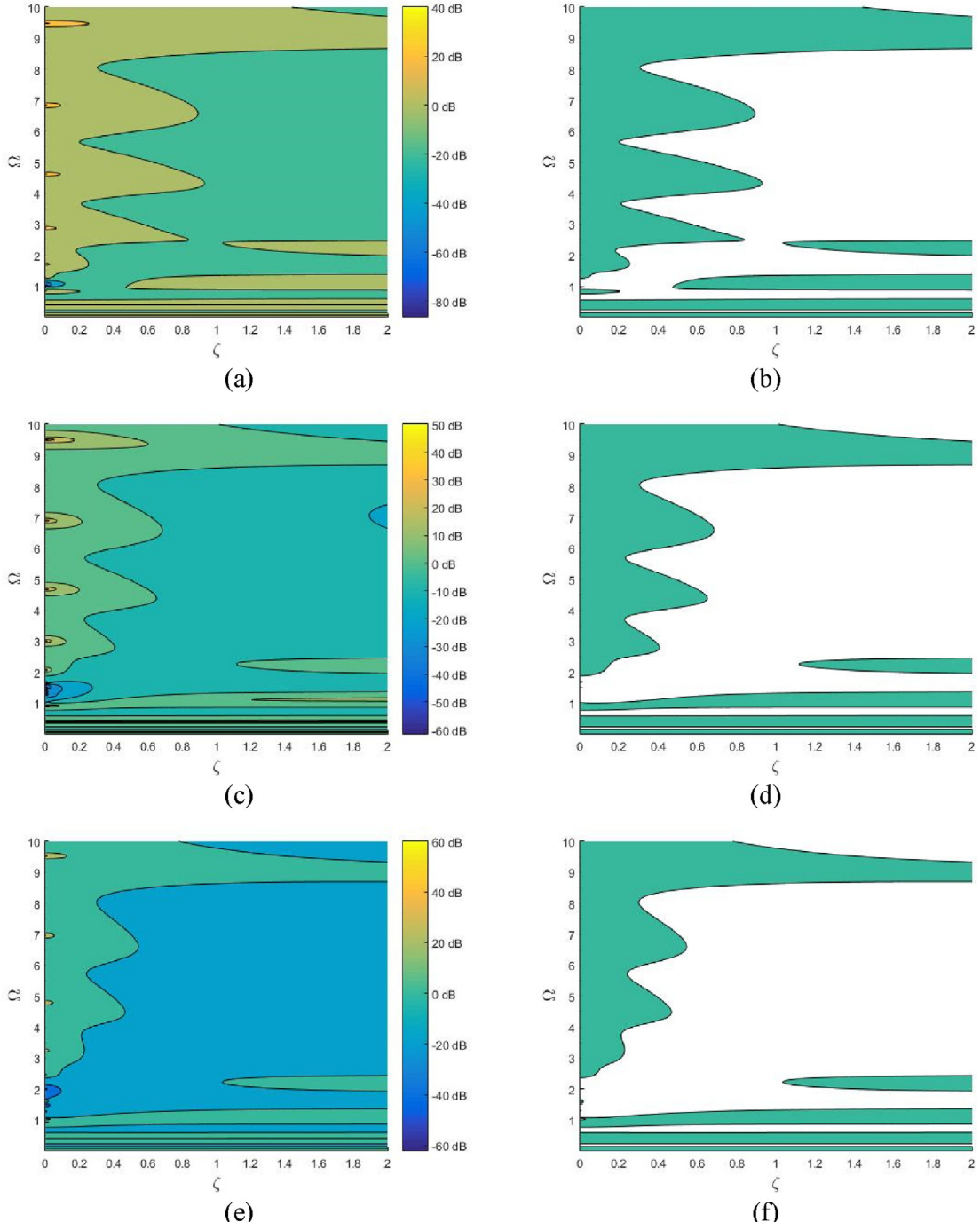


Fig. 8. (a),(c) Contour representation of the transmittance pattern evolution in response to the variation of ζ , (b),(d) image binarization using 0 dB as reference. (a) and (b): $\mu = 0.4$ & $\alpha = 0.6$ & $\delta = 0$; (c) and (d): $\mu = 0.4$ & $\alpha = 0.6$ & $\delta = 0.1$; (c) and (d): $\mu = 0.4$ & $\alpha = 0.6$ & $\delta = 0.2$.

4.2. Effect of the damping ratio ζ

Damping is an important factor that affects the dynamic response of mechanical systems. The damping effect on traditional tuned-mass damper systems has been previously studied and an analytical expression for the optimum damping ratio has been derived [44]. However, the existing literature is concerned primarily with the tuned-mass damper attached to a structure that is modelled as a single-degree-of-freedom system. These simple systems are modelled with lumped parameters, and two fixed points in the frequency response pattern are observed, which mathematically correspond to the two stationary solutions that are independent of the damping ratio. The optimum value of the damping ratio can thus be analytically determined to minimize the maximum frequency response.

The problem in the current study is more complicated. First, the main structure is assumed to be a beam modelled with distributed parameters. Second, rather than a single local resonator (i.e., a tuned-mass damper), multiple local resonators are attached to the host beam at different places. Due to the complexity of this problem, an explicit solution for the optimum value of the damping ratio is difficult to obtain (and likely does not exist). Thus, a numerical parametric study is conducted to investigate the effect of the damping ratio on the dynamic response of the graded metamaterial beam.

For $\mu = 0.4$ and $\alpha = 0.6$, using the criteria in Eqs.(26) and (27), and based on the parametric study presented in Section 4.1, the optimal interval for tuning the natural frequency spacing δ can be obtained. In the following study, the effect of the damping ratio is analyzed by fixing $\delta = 0.1$ which falls into the optimal interval $-0.096 = \delta_l < \delta < \delta_u = 0.183$.

Fig. 8 shows the transmittance pattern as the damping ratio ζ changes. In particular, **Fig. 8(a)** and (b) correspond to $\delta = 0$, i.e., a conventional metamaterial beam with uniform local resonators. In contrast, **Fig. 8(c)** and (d) correspond to a graded metamaterial beam with $\delta = 0.1$. The attenuation regions for the two cases are denoted in **Fig. 8(b)** and (d) by unshaded areas. Similar to the study presented in the previous section, it is observed that the width of the attenuation region of the graded metamaterial beam is increased compared to the conventional one (with uniform local resonators). It is also observed that increasing ζ increases the width of the attenuation region. These observations conform with the existing literature [45,46].

The qualitative analysis only reveals the effect of the damping ratio on the width of the attenuation region. Though **Fig. 8** (a) and (c) provide information about the attenuation strength over the entire spectrum, only a rudimentary identification from the 2D contour plots is possible. To get detailed insights about the attenuation strength within the attenuation regions, **Fig. 9** plots the transmittance responses of the graded metamaterial beam at specific values of ζ . The shaded areas denote the dominant attenuation regions. Similar to **Fig. 8**, it is observed that increasing the damping ratio increases the width of the attenuation region. However, increasing the damping ratio reduces the attenuation strength. In particular, the larger the damping ratio, the shallower the transmittance “valley” (i.e., the attenuation region).

Using the figures of merit, **Fig. 10** quantitatively evaluates the vibration suppression performance of the graded metamaterial beam. From **Fig. 10(a)**, it is observed that with increasing ζ , the bandwidth of the dominant vibration attenuation region Ω_D first increases then decreases. The bandwidth Ω_D reaches the maximum when $0.684 < \zeta < 1.116$. **Fig. 10(b)** reveals the effect of ζ on the lower bound of the dominant vibration attenuation region. In particular, for low-frequency vibration suppression, ζ should be below 1.116. **Fig. 10(c)** presents the variations of τ_{\min} and τ_{avg} with changing ζ . The frequency range of interest (i.e., $[\Omega_A, \Omega_B]$) is the dominant attenuation region that can be determined from **Fig. 10(b)**. It is observed that as ζ increases, τ_{\min} monotonically decreases, while τ_{avg} first increases then decreases. Since a large damping ratio is difficult to achieve in traditional materials and mechanical systems, $\zeta = 0.684$ can be considered as the optimal damping ratio for this case.

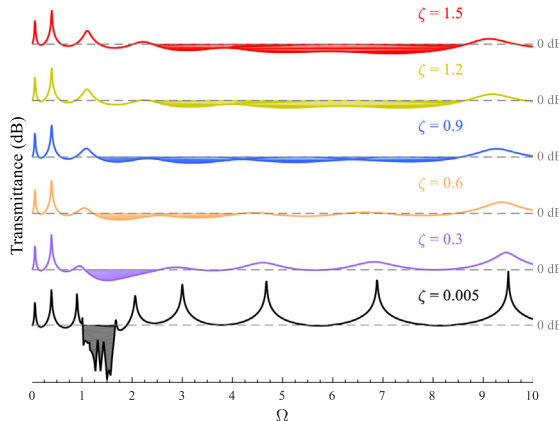


Fig. 9. Transmittance responses of the metamaterial beam with $\mu = 0.4$, $\alpha = 0.6$ and $\delta = 0.1$ for different ζ . The color-filled area denotes the dominant attenuation region.

To reveal the advantages of the proposed strategy, we compare it with another conventional idea inspired from the mechanism of traditional tuned mass dampers. The conventional idea is to attach multiple vibration absorbers to a plain beam, with each absorber targeting a specific resonance peak of the plain beam [47–49]. For $\mu = 0.4$ and $\alpha = 0.6$, the first 6 resonance frequencies of the beam are 0.008, 0.500, 1.399, 2.742, 4.533 and 6.771. Replacing the 6 local resonators by 6 vibration absorbers targeted for the calculated first 6 resonance frequencies of the plain beam, we compare the transmittances responses of the three models, namely, the plain beam, the conventional beam with multiple vibration absorbers attached and the proposed graded metamaterial beam. The damping ratios of the vibration absorbers are set to $\zeta_0 = \sqrt{3\mu/[8(1+\mu)]}$ according to the theory for tuned-mass dampers [44,50]. As shown in Fig. 11, the attenuated region of the conventional plain beam with multiple vibration absorbers attached ranges from 2.603 to 8.617. For the proposed graded metamaterial beam, the attenuated region is slightly widened and ranges from 1.259 to 8.487. It is observed from Fig. 11, the transmittance response of the graded metamaterial beam is obviously flatter than the conventional plain beam with multiple vibration absorbers attached. In addition, the phenomenon presented in Fig. 11 can be explained by the theory from [41]: an appropriate system damping leads to merging of the multiple vibration attenuation regions, resulting in the formation of a broadband frequency range for vibration attenuation. Therefore, the idea of introducing frequency spacing between local resonators and the idea of introducing appropriate dissipative components presented in [41] can be combined to significantly improve the broadband capability for vibration attenuation.

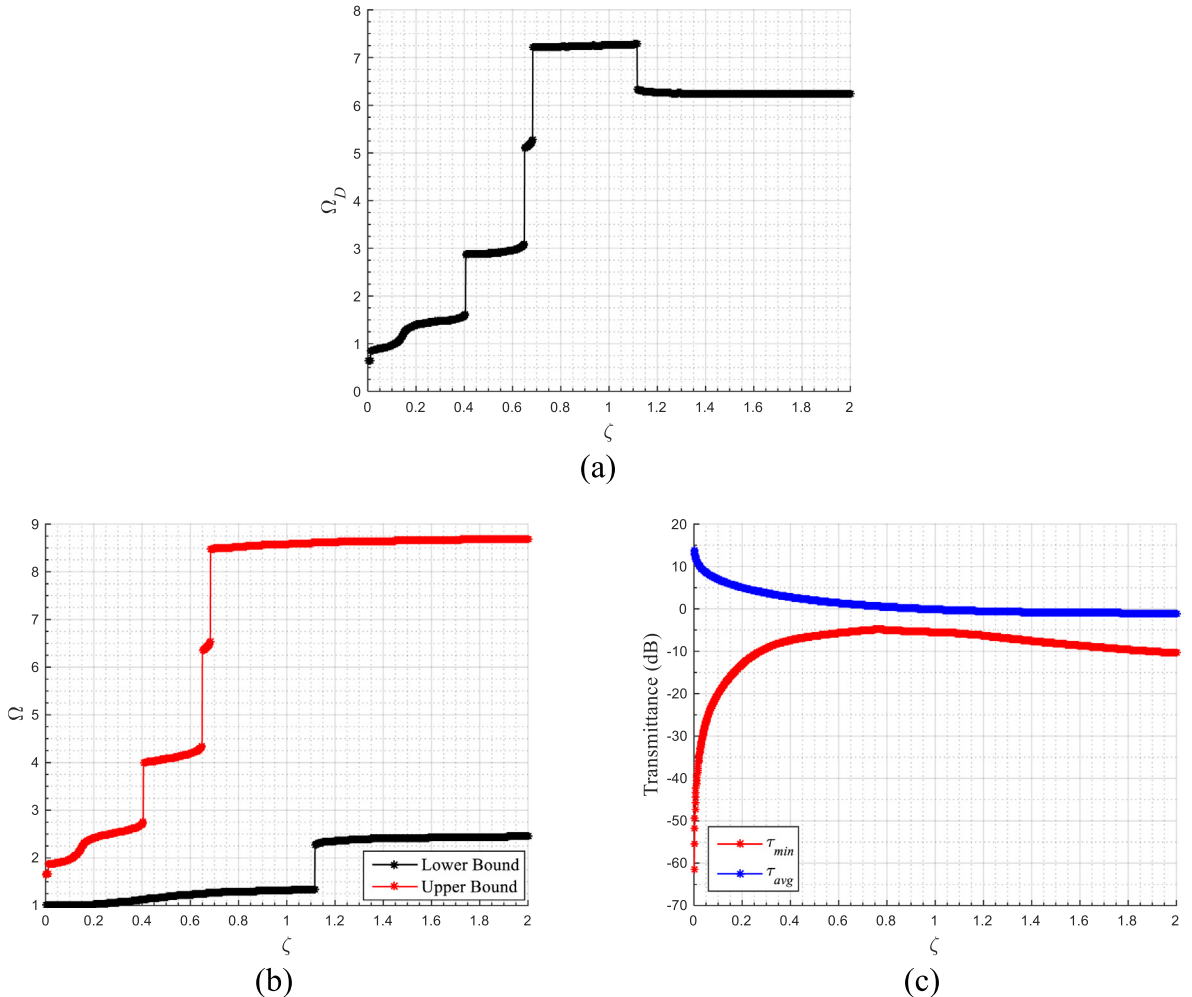


Fig. 10. Evolutions of (a) the bandwidth of the dominant attenuation region, Ω_D , (b) lower and upper bounds of the dominant attenuation region, (c) attenuation indexes (τ_{min} & τ_{avg}) of the dominant attenuation region with the change of ζ , for the graded metamaterial beam with $\mu = 0.4$, $\alpha = 0.6$ and $\delta = 0.1$.

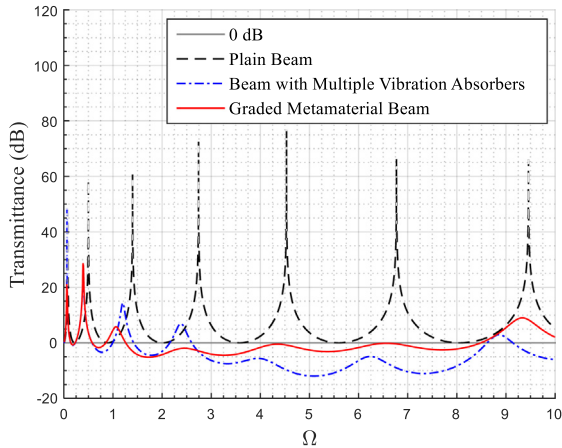


Fig. 11. Comparison of the transmittance responses of the plain beam, the plain beam with multiple vibration absorbers tuned to the beam's resonance frequencies and the graded metamaterial beam with $\delta = 0.1$ and $\zeta = 0.684$.

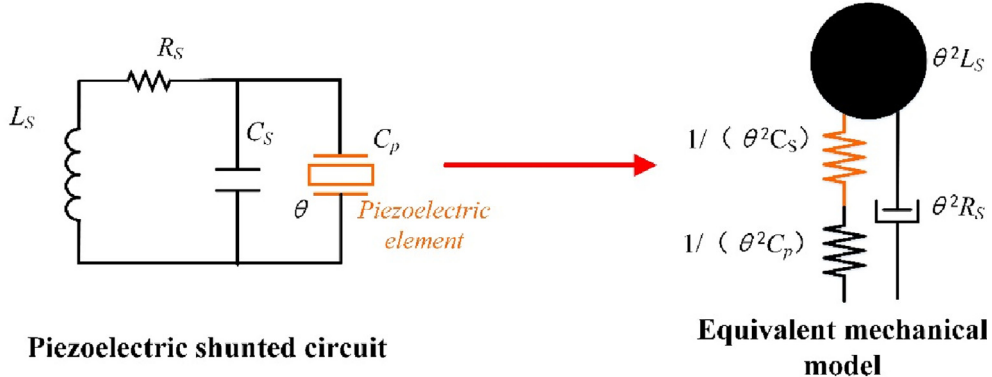


Fig. 12. Equivalence between a piezoelectric shunted circuit and a mass-spring model. L_S , C_S and R_S are the inductance, capacitance and resistance, respectively. C_p is the internal capacitance of the piezoelectric element and θ is the electromechanical coupling coefficient.

5. Finite element case study

5.1. Mechanism explanation

The key to realize the proposed graded metamaterial beam with the developed strategy lies in the implementation of the local resonators with readily tunable stiffness and damping ratio. However, it is difficult to achieve this using solely mechanical structures. Using a structure integrated with shunted piezoelectric patches provides a potential solution by forming the local resonance in the electrical circuit. With the piezoelectric effect, an electrical resonance has been proved to have a similar effect on the hosting structure as a vibration absorber [43–45]. As the governing equations of both the piezoelectric shunted circuit shown in Fig. 12 and the mass-spring system have exactly the same second-order differential form, an inductance shunted piezoelectric circuit can be equivalently represented by a mass-spring-damper system [51,52]. It is worth mentioning that the example demonstrated in Fig. 12 assumes that the piezoelectric element operates in the 33-mode [53].

Due to the ease of implementation, we often design piezoelectric beams to operate in the 31-mode [54] for which an inductance is equivalent to a moment of inertia and a capacitance is equivalent to an inverse torsional spring stiffness. It should be noted that the value of the capacitance is not equal to the stiffness of the torsional spring. A detailed mathematical formulation of such kind of system can be referred to [20]. In the following study, we adopt the 31-mode for the design of the piezoelectric metamaterial beam in which we can vary the shunted impedance to equivalently alter the torsional stiffness and the damping ratio of the local resonator that is constituted by the shunt circuit. The following case study aims to qualitatively capture the main conclusions from the theory of the graded metamaterial beam described in Section 2.

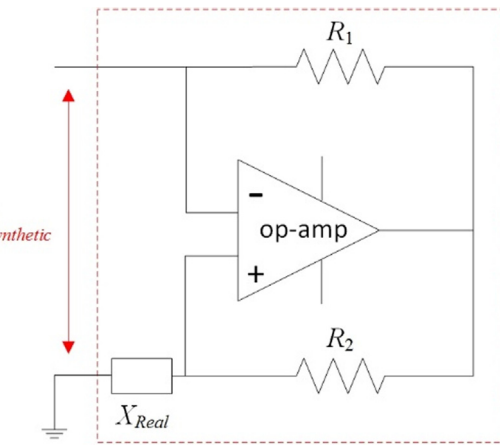


Fig. 13. Schematic of a synthetic shunt circuit.

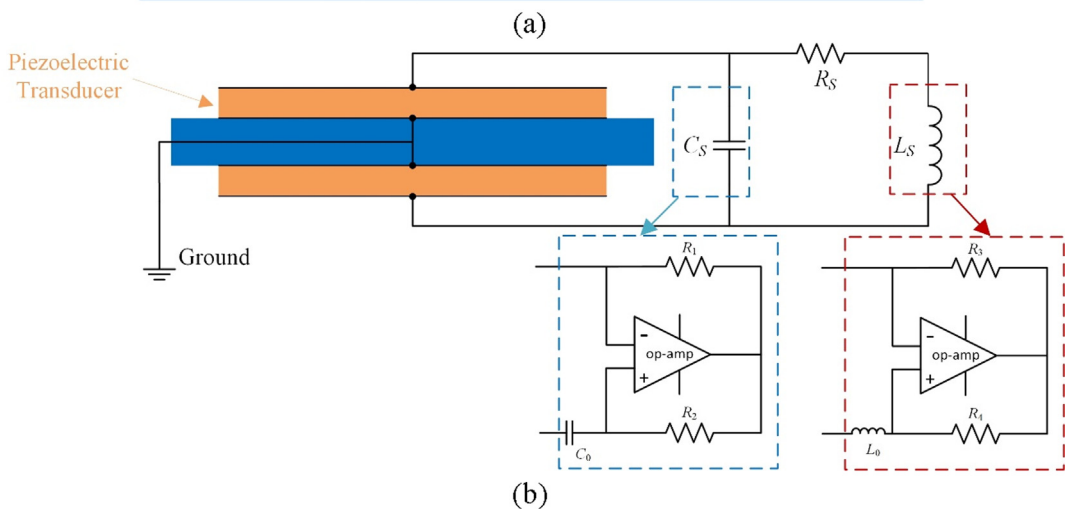
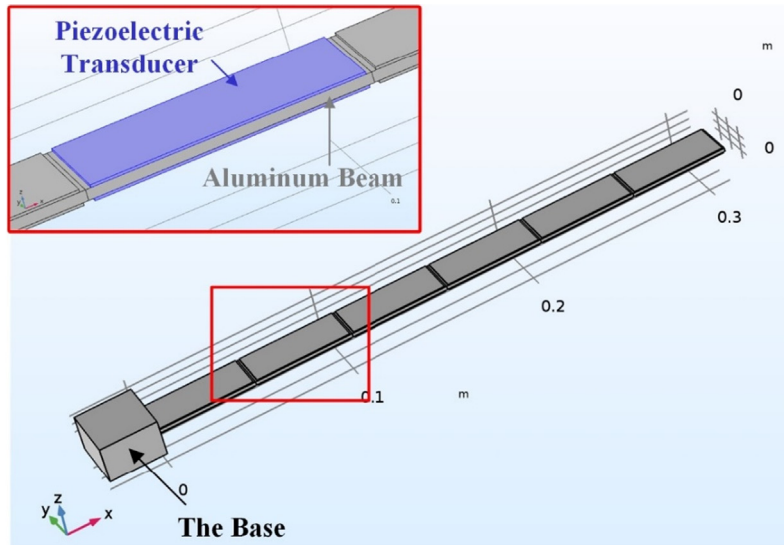


Fig. 14. (a) Finite element model of the piezoelectric metamaterial beam in COMSOL Multiphysics, (b) schematic of a single cell of the graded piezoelectric metamaterial beam shunted with synthetic circuit.

5.2. Synthetic shunt circuit

In this section, the synthetic shunt circuit (shown in Fig. 13) used to achieve the desired electrical impedance, i.e., capacitance/inductance/resistance, is described. The operational amplifier (op-amp) plays a key role in the realization of the synthetic shunt circuit. Based on the characteristics of an ideal op-amp, the equivalent electrical impedance of this synthetic circuit can be derived as:

$$X_{\text{Synthetic}} = -\frac{R_2}{R_1} X_{\text{Real}} \quad (28)$$

The equivalent impedance depends on the ratio of R_2/R_1 . In the physical implementation, due to the non-idealities of practical op-amps, the synthetic circuit would unavoidably introduce undesired noise and additional parasitic elements. Fortunately, the excessive noise and parasitic elements are usually negligible [55–57]. Consequently, no additional electric elements besides the desired impedance need to be taken into account in the theoretical modelling of the synthetic circuit.

5.3. Piezoelectric metamaterial beam

Fig. 14(a) shows the finite element model of the piezoelectric metamaterial beam developed using COMSOL. The geometric and material parameters of this piezoelectric metamaterial beam are listed in Table 1. It consists of a set of piezoelectric transducers periodically bonded onto a host beam. The top and the bottom surfaces of each piezoelectric transducer are emulated as two electrodes. The two electrodes are connected to a synthetic circuit exhibiting electrical resonance. The interface circuits shunted to the piezoelectric transducers are implemented by using the Electrical Circuit Module of COMSOL. Fig. 14(b) shows the details of a single cell of the graded piezoelectric metamaterial beam shunted with the synthetic circuit. Each piezoelectric transducer is shunted to a capacitance and an inductance in parallel.

According to the electro-mechanical analogies, a capacitor, inductor, or resistor in the electrical system can be regarded as a compliance, mass, or damper in the mechanical system respectively. In the analysis, identical inductances are used to ensure the equivalent masses of local resonators are identical. The value of the capacitance shunted to each piezoelectric transducer is different to give the “graded” feature. It should be noted that electrical capacitance is equivalent to mechanical compliance. Since the criteria derived in Section 3 only propose a certain spacing range to avoid any overtuning and a constant frequency spacing is not a necessary condition, a constant capacitance spacing is adopted as it is relatively easy to

Table 1

Geometric and materials parameters of the unit cell of the piezoelectric metamaterial beam.

Geometric Parameters		Material Parameters	
<i>Host Beam - Aluminum</i>			
Length	52 mm	Material Density	2700 kg/m ³
Width	20 mm	Young's Modulus	70 GPa
Thickness	2 mm		
<i>Piezoelectric Transducer – PZT-5A</i>			
Length	50 mm	Material Density	7750 kg/m ³
Width	20 mm	Young's Modulus	66 GPa
Thickness	0.5 mm	Strain coefficient	-12.5C/m ²
			Permittivity component at constant strain
			1.32813 × 10 ⁻⁸ F/m

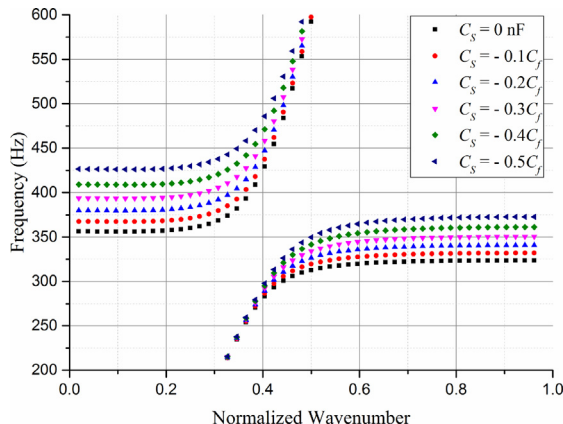


Fig. 15. Band structures of the uniform piezoelectric metamaterial beam for different capacitance values, $C_f = 24\text{nF}$.

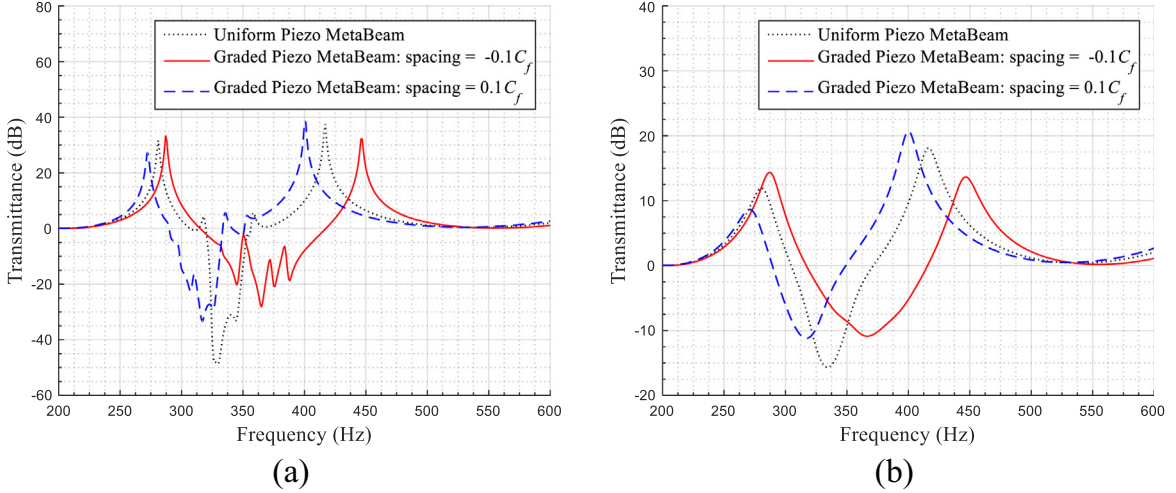


Fig. 16. Comparison of the transmittances of the conventional and the graded piezoelectric metamaterial beams (a) $R_s = 100\Omega$, (b) $R_s = 1000\Omega$.

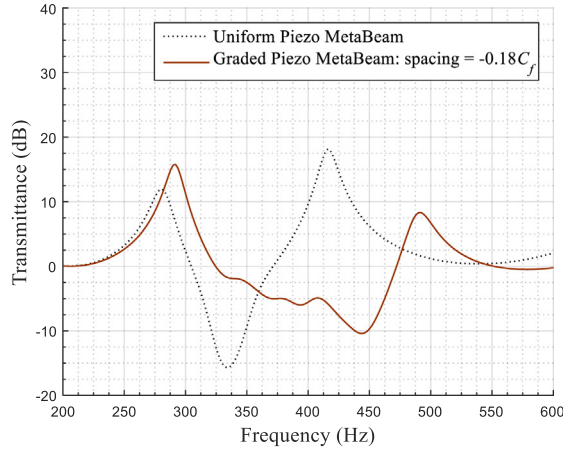


Fig. 17. Transmittance of graded piezoelectric metamaterial beam with a capacitance spacing of $-0.18C_f$.

implement and control in practice. A negative or positive capacitance spacing implies that the natural frequencies of the electric resonators are tuned in the ascending or descending order respectively. When all the capacitances shunted to the piezoelectric transducers are tuned to be identical, a uniform piezoelectric metamaterial beam without "graded" feature is obtained. Fig. 15 shows the band structures of the uniform piezoelectric metamaterial beam shunted to capacitances of different values. It is observed that the band gap of the piezoelectric metamaterial beam can be controlled by changing the value of the shunted capacitance.

For $R_s = 100\Omega$, i.e., under a small damping condition, Fig. 16(a) compares the transmittances of the piezoelectric metamaterial beams shunted with identical and graded capacitances. The conventional metamaterial beam shunted without capacitances (i.e., $C_s = 0 \text{ nF}$) generates a vibration attenuation region from 319.8 Hz to 356.3 Hz. For the piezoelectric metamaterial beam with graded capacitances that are tuned in the descending order with the spacing of $-0.1C_f$ (i.e., the natural frequencies of the electrical resonators are in the ascending order), a vibration attenuation region from 315.1 Hz to 414.7 Hz is generated. The vibration attenuation bandwidth of the graded metamaterial beam is 99.6 Hz which indicates a 172.8% enlargement as compared to the conventional one (36.5 Hz). Moreover, the lower bound of the vibration attenuation region is decreased slightly. These observations agree well with the predictions from the theoretical model developed in Section 2. Similarly, the graded metamaterial beam with resonators tuned in the descending order with the capacitance spacing $0.1C_f$ produces a vibration attenuation region from 289.9 Hz to 333.5 Hz with a bandwidth of 43.6 Hz. Though in this case the bandwidth is not significantly increased compared to the conventional metamaterial beam, the lower bound of the vibration suppression region is reduced from 319.8 Hz to 289.9 Hz, which is favorable for low-frequency vibration suppression.

Fig. 16(b) shows the transmission response with the shunted resistances R_S all tuned to 1000Ω . It is observed that increasing the value of the resistance flattens the transmission response, implying that increasing the resistance is equivalent to increasing the damping of the resonator. The use of the synthetic shunt circuit thus provides an easy way to tune the damping of the electromechanical system, which is difficult to achieve in purely mechanical systems. Under a strong-damping condition, it is noted that the difference between the maximum attenuation strengths of the graded and conventional metamaterial beams becomes smaller. For $R_S = 1000\Omega$, **Fig. 17** shows the transmittance of the graded piezoelectric metamaterial beam with an increased capacitance spacing $-0.18C_f$. It is observed that under the strong-damping condition, a large capacitance spacing can be used for obtaining a relatively wide vibration attenuation region from 324.6 Hz to 472.1 Hz with a bandwidth of 147.5 Hz.

6. Conclusions

In this paper, a graded metamaterial structure consisting of a series of local resonators with different natural frequencies attached to a plain beam has been studied. The spectral element method has been successfully adopted to model the proposed system and verified using the finite element method. Several figures of merit have been defined to enable a quantitative evaluation of the vibration suppression performance of the graded metamaterial from the perspective of the bandwidth of the dominant attenuation region, the maximum attenuation strength and the spectral-averaged attenuation strength. A design strategy has been proposed to tune the local resonators with slightly different natural frequencies to produce a wide attenuation region. Explicit expressions for the critical lower and upper bounds for the frequency spacing between the resonators have been derived. The proposed strategy and criteria have been confirmed through a series of parametric studies. A piezoelectric metamaterial beam has been developed to implement the proposed design strategy. The FEM simulation results have validated the main conclusions of the developed theory: following the proposed strategy, properly tuning the capacitance spacing for each transducer yields greater than 150% enlargement of the attenuation bandwidth compared to the conventional case.

CRediT authorship contribution statement

Guobiao Hu: Investigation, Writing - original draft, Formal analysis, Validation, Software. **Andrew C. M. Austin:** Conceptualization, Methodology, Supervision, Writing - review & editing. **Vladislav Sorokin:** Conceptualization, Methodology, Supervision, Project administration, Writing - review & editing. **Lihua Tang:** Supervision, Writing - review & editing.

Acknowledgement

This work is financially supported by the Ideas Day Seed Fund from the Faculty of Engineering of the University of Auckland.

References

- [1] S. Yao, X. Zhou, G. Hu, Investigation of the negative-mass behaviors occurring below a cut-off frequency, *New J. Phys.* 12 (10) (2010) 103025.
- [2] G. Hu, L. Tang, J. Xu, C. Lan, R. Das, Metamaterial with local resonators coupled by negative stiffness springs for enhanced vibration suppression, *J. Appl. Mech.* (2019) 1–27.
- [3] X. Zhang, Z. Liu, Negative refraction of acoustic waves in two-dimensional phononic crystals, *Appl. Phys. Lett.* 85 (2) (2004) 341–343.
- [4] J. Xu, J. Tang, Tunable prism based on piezoelectric metamaterial for acoustic beam steering, *Appl. Phys. Lett.* 110 (18) (2017) 181902.
- [5] S. Chen, G. Wang, Y. Song, Low-frequency vibration isolation in sandwich plates by piezoelectric shunting arrays, *Smart Mater. Struct.* 25 (12) (2016) 125024.
- [6] G. Hu, L. Tang, X. Cui, On the modelling of membrane-coupled Helmholtz resonator and its application in acoustic metamaterial system, *Mech. Syst. Sig. Process.* 132 (2019) 595–608.
- [7] S.W. Zhang, J.H. Wu, Z.P. Hu, Low-frequency locally resonant band-gaps in phononic crystal plates with periodic spiral resonators, *J. Appl. Phys.* (2013) 113(16).
- [8] G. Huang, C. Sun, Band Gaps in a Multiresonator Acoustic Metamaterial, *J. Vibr. Acoust. Trans. Asme* 132 (3) (2010) 031003.
- [9] Q. Li, Z. He, E. Li, Dissipative multi-resonator acoustic metamaterials for impact force mitigation and collision energy absorption, *Acta Mech.* (2019) 1–31.
- [10] Y. Xiao, J. Wen, X. Wen, Longitudinal wave band gaps in metamaterial-based elastic rods containing multi-degree-of-freedom resonators, *New J. Phys.* 14 (3) (2012) 033042.
- [11] H. Chen, X. Li, Y. Chen, G. Huang, Wave propagation and absorption of sandwich beams containing interior dissipative multi-resonators, *Ultrasonics* 76 (2017) 99–108.
- [12] D. Yu, Y. Liu, H. Zhao, G. Wang, J. Qiu, Flexural vibration band gaps in Euler-Bernoulli beams with locally resonant structures with two degrees of freedom, *Phys. Rev. B* 73 (6) (2006) 064301.
- [13] K. Lu, J.H. Wu, L. Jing, D. Guan, Flexural vibration bandgaps in local resonance beam with a novel two-degree-of-freedom local resonance system, *Eur. Phys. J. Appl. Phys.* 77 (2) (2017) 20501.
- [14] W. Zhou, Y. Wu, L. Zuo, Vibration and wave propagation attenuation for metamaterials by periodic piezoelectric arrays with high-order resonant circuit shunts, *Smart Mater. Struct.* 24 (6) (2015) 065021.
- [15] K. Lu, J.H. Wu, L. Jing, N. Gao, D. Guan, The two-degree-of-freedom local resonance elastic metamaterial plate with broadband low-frequency bandgaps, *J. Phys. D Appl. Phys.* 50 (9) (2017) 095104.
- [16] R. Zhu, X. Liu, G. Hu, C. Sun, G. Huang, A chiral elastic metamaterial beam for broadband vibration suppression, *J. Sound Vib.* 333 (10) (2014) 2759–2773.

- [17] Y. Xiao, J. Wen, X. Wen, Broadband locally resonant beams containing multiple periodic arrays of attached resonators, *Phys. Lett. A* 376 (16) (2012) 1384–1390.
- [18] Z. Shuguang, N. Tianxin, W. Xudong, F. Jialu, Studies of band gaps in flexural vibrations of a locally resonant beam with novel multi-oscillator configuration, *J. Vib. Control* 23 (10) (2017) 1663–1674.
- [19] G. Hu, L. Tang, R. Das, Internally coupled metamaterial beam for simultaneous vibration suppression and low frequency energy harvesting, *J. Appl. Phys.* 123 (5) (2018) 055107.
- [20] Li, S., J. Xu, and J. Tang. Adaptive acoustic metamaterial with periodic piezoelectric network. in Active and Passive Smart Structures and Integrated Systems 2017. 2017. International Society for Optics and Photonics.
- [21] G. Hu, L. Tang, R. Das, S. Gao, H. Liu, Acoustic metamaterials with coupled local resonators for broadband vibration suppression, *AIP Adv.* 7 (2) (2017) 025211.
- [22] Y. Xiao, J. Wen, L. Huang, X. Wen, Analysis and experimental realization of locally resonant phononic plates carrying a periodic array of beam-like resonators, *J. Phys. D Appl. Phys.* 47 (4) (2013) 045307.
- [23] M.B. Assouar, J.-H. Sun, F.-S. Lin, J.-C. Hsu, Hybrid phononic crystal plates for lowering and widening acoustic band gaps, *Ultrasonics* 54 (8) (2014) 2159–2164.
- [24] Y. Xiao, J. Wen, G. Wang, X. Wen, Theoretical and experimental study of locally resonant and Bragg band gaps in flexural beams carrying periodic arrays of beam-like resonators, *J. Vib. Acoust.* 135 (4) (2013) 041006.
- [25] O. Thorp, M. Ruzzene, A. Baz, Attenuation and localization of wave propagation in rods with periodic shunted piezoelectric patches, *Smart Mater. Struct.* 10 (5) (2001) 979.
- [26] S. Chen, G. Wang, J. Wen, X. Wen, Wave propagation and attenuation in plates with periodic arrays of shunted piezo-patches, *J. Sound Vib.* 332 (6) (2013) 1520–1532.
- [27] X. Li, Y. Chen, G. Hu, G. Huang, A self-adaptive metamaterial beam with digitally controlled resonators for subwavelength broadband flexural wave attenuation, *Smart Mater. Struct.* 27 (4) (2018) 045015.
- [28] B.-I. Popa, S.A. Cummer, Non-reciprocal and highly nonlinear active acoustic metamaterials, *Nat. Commun.* (2014) 5.
- [29] R. Zhu, Y. Chen, M. Barnhart, G. Hu, C. Sun, G. Huang, Experimental study of an adaptive elastic metamaterial controlled by electric circuits, *Appl. Phys. Lett.* 108 (1) (2016) 011905.
- [30] X. Fang, J. Wen, J. Yin, D. Yu, Wave propagation in nonlinear metamaterial multi-atomic chains based on homotopy method, *AIP Adv.* 6 (12) (2016) 121706.
- [31] X. Fang, J. Wen, B. Bonello, J. Yin, D. Yu, Ultra-low and ultra-broad-band nonlinear acoustic metamaterials, *Nat. Commun.* 8 (1) (2017) 1288.
- [32] Khajehourian, R. and M. Hussein, Nonlinear locally resonant metamaterials: Modeling and dispersion characteristics. Proceedings of Phononics, 2013: p. 180–181.
- [33] M. Brennan, Characteristics of a wideband vibration neutralizer, *Noise Control Engineering Journal* 45 (5) (1997) 201–207.
- [34] A. Banerjee, R. Das, E.P. Calius, Frequency graded 1D metamaterials: A study on the attenuation bands, *J. Appl. Phys.* 122 (7) (2017) 075101.
- [35] V.S. Sorokin, J.J. Thomsen, Eigenfrequencies and eigenmodes of a beam with periodically continuously varying spatial properties, *J. Sound Vib.* 347 (2015) 14–26.
- [36] V.S. Sorokin, Effects of corrugation shape on frequency band-gaps for longitudinal wave motion in a periodic elastic layer, *J. Acoust. Soc. Am.* 139 (4) (2016) 1898–1908.
- [37] Y. Zhang, Eigenfrequency computation of beam/plate carrying concentrated mass/spring, *J. Vib. Acoust.* 133 (2) (2011) 021006.
- [38] Lee, U., Spectral Element Method in Structural Dynamics. 2009.
- [39] H. Sun, X. Du, P.F. Pai, Theory of metamaterial beams for broadband vibration absorption, *J. Intell. Mater. Syst. Struct.* 21 (11) (2010) 1085–1101.
- [40] C. Sugino, S. Leadenham, M. Ruzzene, A. Erturk, On the mechanism of bandgap formation in locally resonant finite elastic metamaterials, *J. Appl. Phys.* 120 (13) (2016) 134501.
- [41] Y. Chen, M. Barnhart, J. Chen, G. Hu, C. Sun, G. Huang, Dissipative elastic metamaterials for broadband wave mitigation at subwavelength scale, *Compos. Struct.* 136 (2016) 358–371.
- [42] C. Hodges, J. Woodhouse, Vibration isolation from irregularity in a nearly periodic structure: theory and measurements, *J. Acoust. Soc. Am.* 74 (3) (1983) 894–905.
- [43] M.I. Hussein, M.J. Leamy, M. Ruzzene, Dynamics of phononic materials and structures: Historical origins, recent progress, and future outlook, *Appl. Mech. Rev.* 66 (4) (2014) 040802.
- [44] H.C. Tsai, G.C. Lin, Optimum tuned-mass dampers for minimizing steady-state response of support-excited and damped systems, *Earthquake Eng. Struct. Dyn.* 22 (11) (1993) 957–973.
- [45] A.D. Nashif, D.I. Jones, J.P. Henderson, *Vibration Damping*, John Wiley & Sons, 1985.
- [46] C. Beards, *Structural Vibration: Analysis and Damping*, Elsevier, 1996.
- [47] T. Igusa, K. Xu, Vibration control using multiple tuned mass dampers, *J. Sound Vib.* 175 (4) (1994) 491–503.
- [48] R. Jacquot, Optimal dynamic vibration absorbers for general beam systems, *J. Sound Vib.* 60 (4) (1978) 535–542.
- [49] H. Özgür, B. Candir, Suppressing the first and second resonances of beams by dynamic vibration absorbers, *J. Sound Vib.* 111 (3) (1986) 377–390.
- [50] M.J. Brennan, Some recent developments in adaptive tuned vibration absorbers/neutralisers, *Shock Vib.* 13 (4, 5) (2006) 531–543.
- [51] J. Liang, W. Liao, Impedance modeling and analysis for piezoelectric energy harvesting systems, *IEEE/ASME Trans. Mechatron.* 17 (6) (2012) 1145–1157.
- [52] Y. Yang, L. Tang, Equivalent Circuit Modeling of Piezoelectric Energy Harvesters, *J. Intell. Mater. Syst. Struct.* 20 (18) (2009) 2223–2235.
- [53] S. Priya, D.J. Inman, *Energy Harvesting Technologies*, Springer, New York, 2009.
- [54] A. Erturk, D.J. Inman, A distributed parameter electromechanical model for cantilevered piezoelectric energy harvesters, *J. Vib. Acoust. Trans. Asme* 130 (4) (2008) 041002.
- [55] H. Ji, J. Qiu, J. Cheng, D. Inman, Application of a negative capacitance circuit in synchronized switch damping techniques for vibration suppression, *J. Vib. Acoust.* 133 (4) (2011) 041015.
- [56] J. Tang, K. Wang, Active-passive hybrid piezoelectric networks for vibration control: comparisons and improvement, *Smart Mater. Struct.* 10 (4) (2001) 794.
- [57] B. De Marneffe, A. Pneumont, Vibration damping with negative capacitance shunts: theory and experiment, *Smart Mater. Struct.* 17 (3) (2008) 035015.